12-1995

Hybrid treatment of spatio-temporal behavior in surface reactions with coexisting immobile and highly mobile reactants

Michael Joseph Tammaro
Iowa State University

M. Sabella
Iowa State University

James W. Evans
Iowa State University, evans@ameslab.gov

Hybrid treatment of spatio-temporal behavior in surface reactions with coexisting immobile and highly mobile reactants

Abstract
For surface reactions on single-crystal substrates which involve highly mobile adspecies, there is a vast separation in natural time and length scales. Adspecies hop rates can be many orders of magnitude larger than rates for other processes. Strong spatial correlations or ordering can exist on the atomic scale, while spatial pattern formation occurs on a macroscopic scale due to high diffusivity. An efficient analysis of such systems is provided by a "hybrid treatment" which we apply here to the monomer-dimer surface reaction model in the case of coexisting immobile dimer adspecies and highly mobile monomer adspecies. Specifically, we combine a mean-field treatment of the "randomized" mobile adspecies, and a lattice-gas description of the immobile adspecies. Monte Carlo simulations then reveal bistability and "critical" bifurcation phenomena, while precisely accounting for the influence of correlations in the immobile adspecies distribution. A corresponding analysis of the evolution of macroscopic spatial inhomogeneities is achieved through parallel simulation of the distributed macroscopic points with distinct correlated states and adspecies coverages. These simulations are appropriately coupled to describe diffusive mass transport of the mobile adspecies. In this way, we examine for this model the propagation and structure of chemical waves, corresponding to interface between bistable reactive states, and thereby determine the relative stability of these states.

Disciplines
Biological and Chemical Physics | Mathematics | Physics

Comments
The following article appeared in *Journal of Chemical Physics* 103,23 (1995): 10277 and my be found at doi: 10.1063/1.469929.

Hybrid treatment of spatio-temporal behavior in surface reactions with coexisting immobile and highly mobile reactants

M. Tammaro, M. Sabella, and J. W. Evans

Citation: The Journal of Chemical Physics **103**, 10277 (1995); doi: 10.1063/1.469929
View online: http://dx.doi.org/10.1063/1.469929
View Table of Contents: http://scitation.aip.org/content/aip/journal/jcp/103/23?ver=pdfcov
Published by the AIP Publishing

Hybrid treatment of spatio-temporal behavior in surface reactions with coexisting immobile and highly mobile reactants

M. Tammaro
Ames Laboratory and Department of Physics, Iowa State University, Ames, Iowa 50011

M. Sabella
Ames Laboratory, Iowa State University, Ames, Iowa 50011

J. W. Evans
Ames Laboratory and Department of Mathematics, Iowa State University, Ames, Iowa 50011

(Received 31 July 1995; accepted 13 September 1995)

For surface reactions on single-crystal substrates which involve highly mobile adspecies, there is a vast separation in natural time and length scales. Adspecies hop rates can be many orders of magnitude larger than rates for other processes. Strong spatial correlations or ordering can exist on the atomic scale, while spatial pattern formation occurs on a macroscopic scale due to high diffusivity. An efficient analysis of such systems is provided by a ''hybrid treatment'' which we apply here to the monomer–dimer surface reaction model in the case of coexisting immobile dimer adspecies and highly mobile monomer adspecies. Specifically, we combine a mean-field treatment of the ''randomized'' mobile adspecies, and a lattice-gas description of the immobile adspecies. Monte Carlo simulations then reveal bistability and ''critical'' bifurcation phenomena, while precisely accounting for the influence of correlations in the immobile adspecies distribution. A corresponding analysis of the evolution of macroscopic spatial inhomogeneities is achieved through parallel simulation of the distributed macroscopic points with distinct correlated states and adspecies coverages. These simulations are appropriately coupled to describe diffusive mass transport of the mobile adspecies. In this way, we examine for this model the propagation and structure of chemical waves, corresponding to interface between bistable reactive states, and thereby determine the relative stability of these states. © *1995 American Institute of Physics.*

I. INTRODUCTION

The interplay between nonlinear chemical reaction kinetics and the diffusion of reactants can produce a rich variety of spatial pattern formation.[1] Traditionally these phenomena are described by mean-field (MF) reaction-diffusion equations which ignore any spatial correlations or ordering in the distribution of reactants.[1] For surface reactions on single crystal substrates,[2,3] this treatment is not strictly justified (even for spatially uniform states) since strong correlations are typically produced either by adspecies interactions, or by the limited mobility of some reactants. Appropriate treatment of these correlations could potentially be provided by lattice-gas (LG) modeling.[4–14] However a basic obstacle is that in many fundamental reactions, including $CO+\frac{1}{2}O_2 \rightarrow CO_2$ and $CO+NO \rightarrow CO_2+\frac{1}{2}N_2$, the surface hop rates for the most mobile adspecies (CO and NO) are many orders of magnitude higher than the rates for other processes[2,3] (adsorption, desorption, reaction, and hopping of relatively immobile adsorbed O). This great separation of time scales makes direct LG simulation difficult. Perhaps even more problematic is the fact that these large hop rates establish spatial patterns on a macroscopic length scale, which coexist with ordering on the vastly shorter atomic length scale of the spatial correlations. Both of these phenomena must be described *simultaneously*. (For the systems of interest here, there are just these two far-separated length scales, but it is also possible for surface reactions to exhibit turbulence, where one has a continuum of length scales.[1,3])

To efficiently analyze the above type of systems, we adopt a ''hybrid treatment'' which involves a full LG description for the time-evolution of the distribution of any (relatively) immobile adspecies, together with a local-equilibrium description of any highly mobile adspecies. Specifically, kinetic Monte Carlo simulations are used to describe the immobile adspecies, and for the case of negligible adspecies interactions considered here, a standard MF treatment is used to describe the highly mobile adspecies. However, if adspecies interactions are significant, a more sophisticated treatment is required to account for correlations in the distribution of the locally equilibrated mobile adspecies. We note that hybrid treatments of surface reactions have been implemented previously.[10] However, they have not been applied to analyze the basic features of bistability and bifurcations in spatially homogeneous systems. Furthermore, they have not been extended to describe of the evolution of macroscopic spatial inhomogeneities. To this end, we have developed a novel technique to analyze such phenomena within a hybrid formalism. This is involves parallel simulation of macroscopically separated points with distinct local adspecies coverages, together with incorporation of coupling between these simulations to describe the diffusive mass transport of the highly mobile adspecies.

In this contribution, we analyze a generic monomer–dimer surface reaction model, described in Sec. II, in the limiting regime of highly mobile monomer adspecies and immobile dimer adspecies. We implement a hybrid treatment using a MF description of the highly mobile locally equilibrated species, and a LG description for the immobile spe-

cies. Monte Carlo simulations, described in Sec. III, reveal MF-type bistability and bifurcation behavior, but with some significant modifications due the influence of correlations in the distribution of immobile adspecies. In Sec. IV, we implement the parallel simulation procedure mentioned above to analyze the propagation and structure of chemical waves, corresponding to the interface between bistable reactive states, thus allowing determination of the relative stability of these states. MF-type ''dynamic-cluster'' approximations for the distribution of immobile adspecies are also shown provide accurate descriptions of hybrid model behavior (see Appendix A).

II. MODEL DESCRIPTION

We first describe a generic LG model for the monomer–dimer (or $A+B_2$) surface reaction. This model mimics the oxidation of CO on single-crystal surfaces, with A corresponding to the highly mobile CO, and B to the relatively immobile O. Below (g) denotes the gas phase, (ad) denotes the adsorbed phase, and E denotes an empty surface site. Then the reaction model includes the following mechanistic steps: (i) A(g) impinges on the surface at rate y_A (per site), adsorbing if a randomly selected site is empty; (ii) B_2(g) impinges randomly on the surface at rate y_B (per site), adsorbing if both sites in a randomly selected adjacent pair are empty; (iii) each pair of A(ad) and B(ad) on adjacent sites reacts at rate k, forming AB(g), which then desorbs leaving an adjacent empty pair; (iv) each A(ad) can spontaneously desorb at rate d, leaving an empty site; (v) B(ad) is assumed to be immobile, but A(ad) attempts to hop to randomly selected adjacent sites at rate h, the hop being successful only if the selected site is empty. Implicitly, the above prescription of rates ignores adspecies interactions. Schematically, one writes

$$A(\mathrm{g})+E\rightarrow A(\mathrm{ad}), \quad B_2(\mathrm{g})+2E\rightarrow 2B(\mathrm{ad}),$$

$$A(\mathrm{ad})+B(\mathrm{ad})\rightarrow AB(\mathrm{g})+2E, \quad A(\mathrm{ad})\rightarrow A(\mathrm{g})+E.$$

Here we normalize impingement rates so that $y_A+y_B=1$, which sets the time scale in the model, and also set $y=y_A$. We also choose the reaction rate $k=1$, but other (nonvanishing) values produce qualitatively similar behavior. We consider only a square lattice of adsorption sites, and focus on behavior in the limit of infinite system size. While our simulation studies are performed on finite systems with periodic boundary conditions, we check that finite-size effects are negligible. (The only exception is in the finite-size scaling analysis in Sec. III B, which exploits finite-size effects.)

From previous studies of this LG model for $d=0$ (*no* A-desorption) with both finite k and infinite k (instantaneous reaction), one finds a stable reactive steady state only for a range $y_1<y<y_2$. There is a continuous transition to a B-poisoned ''adsorbing'' state at $y=y_1$, and a discontinuous transition to an A-poisoned ''adsorbing'' state at $y=y_2$. Also, the stable reactive steady state has a metastable extension above y_2, up to a spinodal point $y=y_s$. For $h=0$ [immobile A(ad)], it has been shown that $y_1=0.391$,[11] $y_2=0.5256$,[9] and $y_s=0.528$ (Ref. 12) for infinite k (instantaneous reaction), and $y_1=0.365$,[13] $y_2=0.432$,[12] and $y_s=0.437$ (Ref. 12) when $k=1$. Introducing diffusion of A(ad) (so now $h>0$) has little effect on the B-poisoning transition.[14,15] However, it is expected to greatly enhance metastability[8,15–17] of the reactive state for $y>y_2$, and in fact to increase the width of the metastable window $\Delta y=y_s-y_2$. As a result, most simulation estimates[14] of y_2 for $h>0$ have been corrupted since the system tends to become trapped in this metastable reactive state (see Ref. 16). This difficulty can be avoided by using the ''constant-coverage ensemble'' simulation technique,[9] which we have applied here to the above LG model for the case $k=1$ (and $d=0$) to show that $y_2=0.4320$, 0.4284, 0.4247, 0.4234, for $h=0$, 1, 2, 4, respectively (cf. Ref. 15).

If $d>0$, then clearly there is no longer a trivial adsorbing A-poisoned state. Nonetheless, it has been shown that a discontinuous transition, between a ''highly reactive'' state, and a ''low reactivity near-A-poisoned'' state, persists for a range of $d>0$. This discontinuous transition disappears at a ''critical value'' of $d=d_c>0$.[5,6,7,17]

In this paper, we are interested in behavior of the above model in the regime of very large h. This is motivated by the observation that the hop rate for CO is many orders of magnitude larger than the other rates in typical CO-oxidation reactions. We attempt to determine behavior in this regime directly with a ''*hybrid model*'' for behavior of the full LG model as $h\rightarrow\infty$. Here we assume that, due to very rapid diffusion, A(ad) is distributed *randomly* on the non-B(ad) sites at all times. Shortcomings of this assumption is discussed below. Thus in the hybrid model for a (macroscopically) spatially uniform system, one tracks the number, N_B, *and* location of all B(ad) on the square lattice of adsorption sites, but only tracks the number, N_A, of A(ad). The hierarchic rate equations for this model are described in Appendix A.

Simulation of this model on a (large) finite lattice of N sites is similar to that of the full LG model above. At each Monte Carlo step, as usual, one randomly selects between adsorption, reaction, etc., with weights determined by the relative rates for these processes. When deciding whether to adsorb or desorb A, or to react a B(ad) with an A(ad), it is necessary to decide whether a chosen non-B(ad) site is occupied by one of the randomly distributed A(ad). We say that such a site is occupied by A(ad) with probability $p=N_A/N_Z$, where $N_Z=N-N_B$ denotes the total number of non-B(ad) sites. (Fluctuations in p are small for a large system). Thus if it is decided to attempt A-adsorption (A-desorption) at a selected non-B(ad) site, such adsorption (desorption) is implemented with probability $1-p$ (p), measuring the probability that the site is empty (occupied by A), and then N_A is incremented by $+1$ (-1). Reaction is treated similarly, if successful requiring N_A to be incremented by -1, N_B by -1, and N_Z by $+1$. Of course, B-adsorption requires N_B be incremented by $+2$, and N_Z by -2.

It should be noted that this hybrid model *assumes* a uniform distribution of A(ad) on all non-B(ad) sites, *even if these sites are topologically disconnected by B(ad)-regions*. For the full LG model, even in the limit of high mobility, there would be fluctuations in A(ad) coverages between such

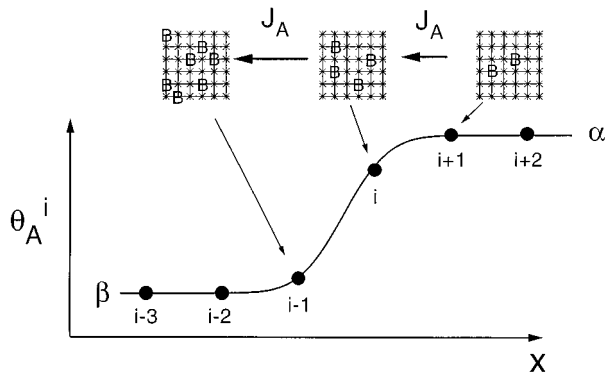

FIG. 1. Schematic of parallel hybrid simulation of generally distinct states of macroscopic points, i, distributed across the front of a propagating chemical wave separating states α and β. Non-B(ad) sites, $*$, are occupied by A(ad) with probability determined by the local coverage, θ_A^i. Simulations are coupled by adjusting θ_A^i to describe diffusive transport of A(ad).

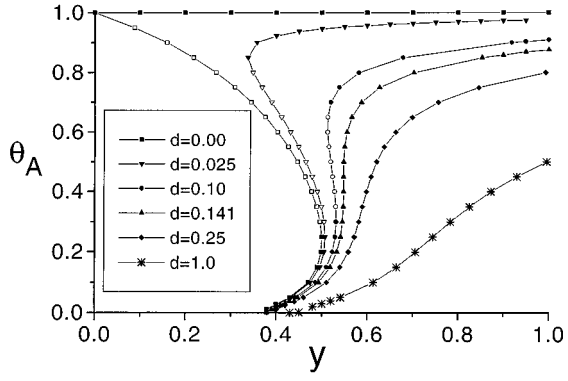

FIG. 2. Steady-state θ_A vs impingement rate, y, for several values of d. For $d<d_c\approx 0.14$, there is bistability. The unstable branches are distinguished by the open plot symbols. These simulations (both standard and CC) were run on 200×200 lattices for 10 000–40 000 Monte Carlo steps (MCS).

disconnected regions. Thus our hybrid model cannot precisely describe the $h\to\infty$ limit of the above LG model. However, we have no reason to expect that the influence of such fluctuations is large.

As noted above, we extend our analysis to systems with spatial inhomogeneity on a macroscopic scale determined by the large diffusion rate of A(ad). Our approach is analogous to the treatment of MF reaction-diffusion (partial differential) equations by the ''method of lines,'' where space is discretized into a set macroscopic points.[18] In the MF treatment, the evolution of coverages at each such point is determined by the appropriate MF rate equations, augmented by a contribution to diffusive flux between adjacent points (which is driven by macroscopic spatial variations in the coverages). However, in the hybrid model, instead of integrating a simple set of MF rate equations at each such macroscopic point, one must perform a separate simulation to describe exactly the distinct local coverages and correlated configurations. Simulations at these individual macroscopic points must be appropriately coupled to describe macroscopic diffusive transport of A. This is indicated schematically in Fig. 1.

In the traditional ''hydrodynamic'' view, description of macroscopic diffusive transport requires determination of the nontrivial collective (or chemical) diffusion coefficient, D_A, for the nonequilibrium state associated with each macroscopic point.[19] The validity of the ''hydrodynamic'' description of mass transport in the type of LG surface reaction models considered here, and the existence (and determination) of associated nontrivial collective diffusion coefficients, has received little attention. For the above LG model, one can, however, say that D_A scales like a^2h, where a denotes the lattice constant. In this work, for simplicity, we implement the simplest description where diffusive transport is described by a constant D_A. However, we also consider a modified description of transport, which accounts for the influence of B(ad) on the diffusion of A(ad).[17]

III. KINETICS AND STEADY STATES FOR SPATIALLY UNIFORM SYSTEMS

A. General features of the phase diagram and kinetics

First we describe simulation results for the steady-state behavior of the hybrid model. Figure 2 shows the variation of the coverage, θ_A, of A(ad) with y, for various d. Here we choose θ_A (instead of θ_B) only by convention. For $d<d_c\approx 0.14$, one finds bistability, i.e., a range of y where a stable low-θ_A state (β) of high reactivity coexists with a stable high-θ_A state (α) of low reactivity. The state α is an A-poisoned ''adsorbing'' state for $d=0$. The states α and β are joined at their spinodal end points by an unstable steady-state branch to form a van der Waals type loop.[5,9] To test for the existence of true bistability, we have checked that if the one perturbs the system from the unstable state by slightly increasing (decreasing) θ_A, it will evolve to the stable state $\alpha(\beta)$ (see Fig. 3). For $d>d_c$, bistability disappears and

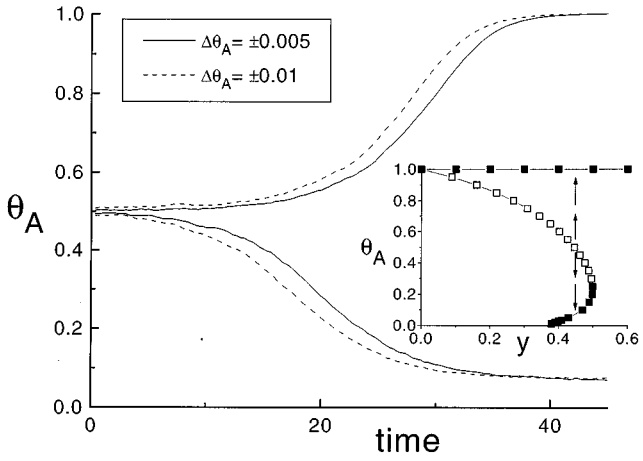

FIG. 3. ''Bistability kinetics'' of the spatially uniform system for $y\approx 0.45$ and $d=0$. Plotted is θ_A vs time for initial states slightly above (below) the unstable steady-state branch. The inset figure is a schematic of this evolution.

there is a unique stable steady state for all y. Thus $d=d_c$ corresponds to a cusp bifurcation,[2] and is the nonequilibrium analog of a critical point.

Conventional simulations, as described in Sec. II, allow analysis of the stable steady states, but not unstable states. However, analysis of the nontrivial unstable steady states (as well as stable steady states) is possible utilizing a ''constant-coverage (CC) ensemble'' approach.[9] This CC approach has previously provided an alternative to other techniques, but in the analysis of unstable states, it is an indispensable tool. The idea is simply to run the simulation maintaining a fixed value of θ_A, say, θ_A^*. As usual, one randomly selects between attempting adsorption, desorption, and reaction events with the appropriate weights. However, now when adsorption is attempted, rather than selecting A with probability y, or B_2 with probability $1-y$, one attempts to deposit A if $\theta_A < \theta_A^*$, or B_2 if $\theta_A > \theta_A^*$. Then the asymptotic fraction of attempts to deposit A gives the corresponding value of y. In this way, we can map out both the stable and unstable steady-state branches. We have checked that finite-size effects are insignificant for the 200×200 site lattices used here, and that CC and conventional simulations give the same results for the stable steady states.

One should in fact expect the occurrence of bistability in the hybrid model for $d<d_c$ (as opposed to a discontinuous transition between α and β states, observed in LG models for $h<\infty$ and $d<d_c$). We have already noted that metastability increases in the LG model with increasing h, and this naturally produces bistability as $h\to\infty$. A more complete understanding of behavior in the LG model with increasing h comes from considering associated nucleation phenomena. Slightly above (below) the discontinuous transition, the area of the critical nucleus required to trigger the formation of the stable $\alpha(\beta)$ state from a metastable $\beta(\alpha)$ background is expected[8] to scale linearly with h. Thus nucleation in the $h\to\infty$ regime requires macroscopic fluctuations, and so bistability is established.

Another feature of the phase diagram in the hybrid model is the continuous B-poisoning transition. This transition occurs at $y=y_1\approx0.3775$ when $d=0$. It has been found for the LG model with $d=h=0$ that this transition falls within the university class of Reggeon field theory and directed percolation,[11] and the same appears to be true for the hybrid model. See Appendix B for a complete discussion.

It is possible to estimate the ''exact behavior'' obtained via simulations for the hybrid model by using MF-type ''dynamic-cluster'' approximations to describe correlations in the distribution of B(ad).[20] These approximations can describe bistability (but not discontinuous transitions), so might be expected to provide a particularly accurate description of hybrid model behavior. We have developed and analyzed the associated rate equations in both the site and pair[13] approximations (see Appendix A). The site approximation neglects all spatial correlations; that is, the distribution of B(ad) on the surface is assumed random. [Recall that the A(ad) are already randomly distributed in this hybrid model.] The site approximation thus corresponds to the standard MF description of the model. However, in the pair approximation, one accounts for correlations in the occupancy by B(ad) of adjacent pairs of sites. The phase diagrams in both approximations are shown in Fig. 4. Both display bistability for $d<d_c\approx0.14$, but only the pair approximation supports a B-poisoning transition. In fact, apart from behavior near the B-poisoning transition, both the site and pair approximations describe quite well the exact phase diagram.

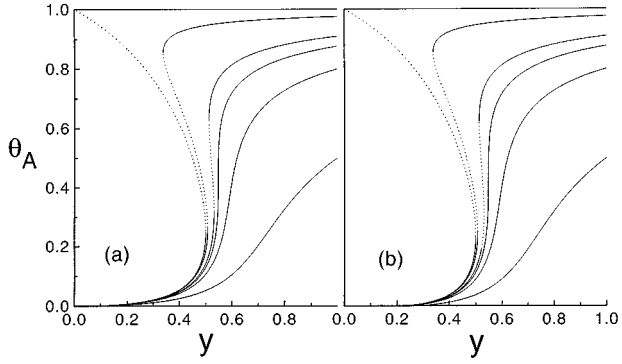

FIG. 4. Steady-state θ_A vs y, from (a) the site approximation; (b) the pair approximation (with the B-poisoning transition at $y\approx0.23$). Apart from the B-poisoning transition there is excellent quantitative agreement between the two approximations and the simulation.

B. The critical point

Another fundamental issue for the hybrid model is the characterization of fluctuation behavior in the vicinity of the critical point which occurs at $d=d_c\approx0.14$ and $y=y_c\approx0.55$. We first note that, for a finite system of N sites, with translational invariance due to periodic boundary conditions, the basic relationship between root-mean-square (rms) coverage fluctuations for adspecies $J=A$ or B, and the associated spatial correlations is

$$\Delta_J=\langle(\theta_J-\langle\theta_J\rangle)^2\rangle^{1/2}=\left[\frac{\Sigma_{\mathbf{l},\mathbf{l}'}C_{JJ}(\mathbf{l},\mathbf{l}')}{N^2}\right]^{1/2}. \tag{1}$$

Here $C_{JJ}(\mathbf{l},\mathbf{l}')$ is the species J pair-correlation function for sites $\mathbf{l}$ and $\mathbf{l}'$, and again N is the size (number of sites) of the system. See Appendix C for a derivation. To elucidate the behavior of the fluctuations, consider first MF behavior associated with a random distribution of adspecies in a finite system. Here we have $C_{JJ}(\mathbf{l},\mathbf{l}')=\langle\theta_J\rangle(1-\langle\theta_J\rangle)\delta_{\mathbf{l},\mathbf{l}'}$ and consequently that $\Delta_J=N^{-1/2}[\langle\theta_J\rangle(1-\langle\theta_J\rangle)]^{1/2}$. So we naturally consider

$$F_J=\frac{N^{1/2}\Delta_J}{[\langle\theta_J\rangle(1-\langle\theta_J\rangle)]^{1/2}}, \tag{2}$$

which is identically unity in the MF case.

In Fig. 5, we show F_A and F_B vs d, for fixed $y=0.55$ close to the critical point, and for systems of different linear sizes L (i.e., $L\times L=N$). These quantities display dramatic maxima which occur in the vicinity of the critical point $d=d_c\approx0.14$. Thus behavior more resembles that of a ''fluctuation-dominated'' critical point in equilibrium theory or in a LG reaction model, rather than MF behavior. In a more comprehensive analysis, for each fixed L, we have found the maximum of F_J as a function of y and d, thus

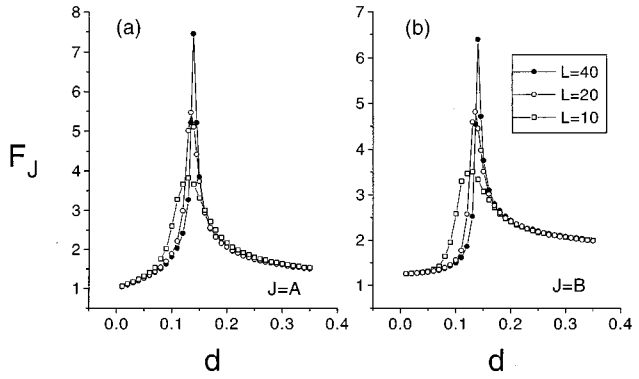

FIG. 5. Normalized rms coverage fluctuations, F_J, vs d, for $y \approx 0.55$, in finite systems of various sizes, N: (a) $J=A$; (b) $J=B$. Dramatic maxima are found for $d \approx d_c$ suggesting that the critical point in the hybrid model is a fluctuation-dominated critical point.

locating the finite size estimate $[y_c(L), d_c(L)]$, of the critical point location, (y_c, d_c). This allows a finite-size-scaling analysis to obtain an estimate of the infinite lattice critical point. Here one assumes[7] that $d_c(L)$ scales with system size as

$$d_c(L) - d_c = aL^{-1/v}, \tag{3}$$

where v is the correlation-length critical exponent. In Fig. 6, we plot $d_c(L)$ against $1/L$. The points for the larger sizes seem to fall on a straight line suggesting that $v=1$ as for the Ising model in two dimensions.[7] This analysis gives an estimate of $d_c = 0.1405 \pm 0.001$. We attempted a similar analysis to determine y_c. The values of $y_c(L)$ saturated too quickly to be fit by a form like Eq. (3), but lead to an estimate $y_c = 0.5470 \pm 0.0002$. It is appropriate here to compare these results with the MF theory (Table I). The critical values of d_c in the MF theories are virtually indistinguishable from the above estimate, although more significant differences are evident in the steady-state values of the coverages.

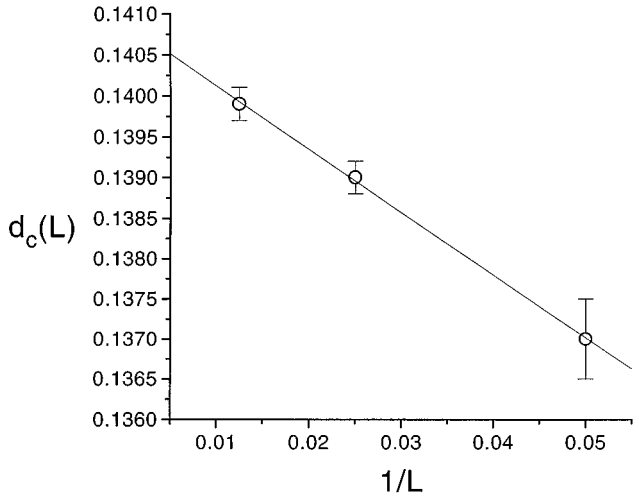

FIG. 6. Finite-size-scaling analysis to locate $d_c = lim_{L\to\infty} d_c(L)$. Results suggest that $d_c = 0.1405 \pm 0.001$.

TABLE I. Comparison of critical points for the MF theories and the simulation. Values of d_c and y_c are equal within the errors of our finite-size-scaling analysis for the simulation.

	d_c	y_c	θ_A^c	θ_B^c
Simulation	0.140 5	0.547 0	0.433	0.128
Pair	0.141 60	0.547 83	0.425 10	0.129 7
Site	0.141 60	0.547 83	0.435 70	0.108 1

One can also perform a more complete analysis of higher order cumulants of the distribution of (fluctuating) coverages. An assessment of the deviation from Gaussian fluctuations is provided by the variation from zero of

$$U_L = \frac{-[\langle \theta_J^4 \rangle - 4\langle \theta_J \rangle \langle \theta_J^3 \rangle - 3\langle \theta_J^2 \rangle^2 + 12\langle \theta_J^2 \rangle \langle \theta_J \rangle^2 - 6\langle \theta_J \rangle^4]}{[3\Delta_J^2]}. \tag{4}$$

In fact, U_L should be maximized at the critical point and take a value of 0.618 if Ising universality applies, as shown[7] for the LG monomer–dimer reaction with $k=\infty$ and $h=0$. We find a maximum of 0.35 ± 0.05 at the critical point for $J=A$ using $L=10$, 20, and 40 (and a lower value for $J=B$). Uncertainty in our statistics precludes definitive conclusion of a deviation from Ising universality.

IV. EVOLUTION OF MACROSCOPIC SPATIAL INHOMOGENEITIES

A. General formalism

We now consider the description of macroscopic spatial phenomena within the hybrid model. To elucidate these phenomena, first consider behavior of the full LG model in the regime where the hop rate, h, of the highly mobile species, A(ad), is large enough to achieve local equilibration, and to justify the use of a local MF treatment A(ad). However, even in this case, there can be variations in adspecies coverages on a macroscopic length scale[2,3] which is of the order of $ah^{1/2}/\kappa^{1/2}$ or $D_A^{1/2}/\kappa$. Here κ denotes an effective rate constant for the overall reaction, a denotes the lattice constant, and D_A the chemical diffusion coefficient (as previously). It is thus spatial variations on a macroscopic length scale of order $D_A^{1/2}$ which we consider below for the hybrid model.

In the standard "hydrodynamic picture," the diffusive flux, $\mathbf{J}_A$, of A(ad) is determined from the collective diffusion coefficient,[19] D_A, via the form $\mathbf{J}_A = -D_A \nabla \theta_A$. In general, D_A depends nontrivially on the local state of the system, however typically it is taken as constant. Thus, we adopt this simplification in our treatment of chemical waves in the hybrid model. However, we also consider one alternative description of transport which falls outside the above general picture. This alternative is motivated by the observation that the above choice of $\mathbf{J}_A$ does not guarantee that $\theta_A + \theta_B \leqslant 1$ at each macroscopic point.[17] To address this shortcoming, we must assess the influence of the presence of B(ad) on A(ad)-diffusion. A "mean-field" estimate of this influence leads us to consider the modified choice[17] $\mathbf{J}_A = -D_A \nabla \theta_A + D_A(\theta_B \nabla \theta_A - \theta_A \nabla \theta_B)$, which enforces the condition $\theta_A + \theta_B \leqslant 1$. The derivation of this result in Appendix D also indicates that correlations in the B(ad)-distribution would

modify $\mathbf{J}_A$, but no simple treatment of these effects is possible. An alternative approach would be to analyze the diffusion of A(ad) on percolating clusters of non-B(ad) sites, using ideas from transport in disordered media. However this is somewhat inconsistent with the imposition in the hybrid model of equal A(ad)-coverages on disconnected clusters on non-B(ad) sites. Consequently we only treat diffusion by the simpler prescriptions above.

For hybrid model parameters in the bistable region, it is possible to consider propagation of chemical waves corresponding to the motion of the interface between stable states α and β. From above, the characteristic length for such waves is of the order $D_A^{1/2}/\kappa$, and it readily follows that the characteristic velocity is of the order $(\kappa D_A)^{1/2}$. Here we consider only planar chemical waves traveling in the x-direction, say, and simulate in parallel the generally distinct local states of the system at discrete macroscopic points, $i=\ldots,-1,\ 0,\ 1,\ldots$ with positions $x=i\,\delta D_A^{1/2}$; here δ is typically chosen around 0.1. We denote the associated local coverages of A(ad) by θ_A^i. To describe the effects of macroscopic diffusion, we must incorporate diffusive mass flow of A between neighboring macroscopic points. Therefore, in addition to running the hybrid model simulations independently at each point, at small time increments, Δt, we make an additional adjustment of the θ_A^i, via $\delta\theta_A^i=-\nabla\cdot\mathbf{J}_A^i\Delta t$, to account for this mass flow. Finally, we note that in order to reduce the number of macroscopic points (and thus the number of simulations we have to run in parallel) required for an accurate description of spatial variations, we use higher order approximations to derivatives in calculating mass flow. For example, when $\mathbf{J}_A=-D_A\nabla\theta_A$, we use

$$-\nabla\cdot\mathbf{J}_A^i=D_A\nabla^2\theta_A^i \approx \frac{-\theta_A^{i+2}+16\theta_A^{i+1}-30\theta_A^i+16\theta_A^{i-1}-\theta_A^{i-2}}{12\delta^2}. \qquad (5)$$

Typical number of macroscopic points used was 100–300 and the lattices used for each macroscopic point had from 100×100 to 200×200 sites.

It is also possible to analyze macroscopic spatial phenomena using the MF-type ''dynamic cluster'' approximations described in Appendix A. Now θ_A and θ_B, as well as probabilities of larger clusters of sites, depend on (macroscopic) position, and one must simply augment the $d\theta_A/dt$ equation with a diffusive term, $-\nabla\cdot\mathbf{J}_A$. [Recall that A(ad) is locally randomized, and that B(ad) does not diffuse.] We also present the results of such analyses below.

B. Chemical wave velocity and equistability points

First, for $d=0$, we determine the variation in the propagation velocity, V, of the interface between states α and β, as y scans the bistable region. Figure 7 shows results from ''parallel simulations'' for both the standard and modified choices of $\mathbf{J}_A$. The results reveal the existence of a point $y=y_e$ where the propagation velocity vanishes. For $y<y_e$, state β displaces α $(V>0)$ and thus β is ''more stable,'' but for $y>y_e$, state α displaces β $(V<0)$ and thus α is ''more stable.'' Thus $y=y_e$ is the ''equistability point'' for states α and β. This is where one would perform a ''kinetic Maxwell construction'' on the van der Waals type loops in Fig. 2 (by analogy with thermodynamic systems). The feature that the location of the equistability point can depend on the description of diffusive mass transport was already recognized from MF reaction-diffusion equation studies.[17] We performed a corresponding analysis using the site- and pair-approximations. Table II shows close agreement between predictions of these approximations and the ''exact'' simulation results. This is perhaps not surprising given the success of these approximations in describing behavior of the hybrid model (away from the B-poisoning transition).

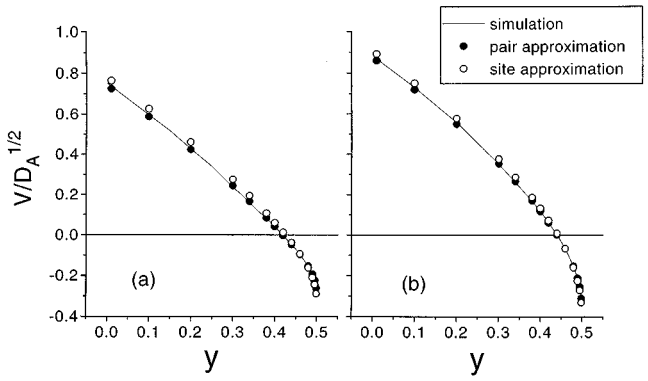

FIG. 7. Propagation velocity of chemical waves, V, vs y, in the bistable region, for $d=0$: (a) standard diffusion, $y_e=0.4404$; (b) modified diffusion, $y_e=0.4185$. The velocity goes to zero at $y=y_e$, the equistability point.

It is appropriate to compare these results with our estimates of behavior in the full LG model [with immobile B(ad), and mobile A(ad) with hop rate h], in the limit as $h\to\infty$. In this LG model, we estimated that the discontinuous transition shifts to about $y=0.423$, as $h\to\infty$ (see Sec. II). Since this discontinuous transition corresponds to the equistability point in the hybrid model, comparison with Table II suggests that the modified description of diffusive transport of A(ad) better describes limiting behavior in the LG model.

Finally, we consider behavior at the equistability point for states α and β for the range $0<d<d_c$. The variation of y_e over this range of d is shown in Table III. Figure 8 shows the corresponding θ_A-concentration profile of the stationary interface or ''kink'' between states α and β. This kink clearly smears out as $d\to d_c$. In order to quantify this ''critical'' roughening,[5,6] we define an interface width, ω, as the dispersion of $(\partial\theta_A/\partial x)$. The results, also shown in Table III, support the expectation that $\omega\to\infty$, as $d\to d_c$, although it is difficult for us to quantify the nature of this divergence.

TABLE II. Comparison of equistability points, y_e, for the MF theories and simulation. Incorporation of B(ad) correlations in the pair approximation produce particularly precise results.

Comparison of equistability points for $d=0$			
	Simulation	Pair	Site
Modified diffusion	0.4185	0.4185	0.4249
Standard diffusion	0.4404	0.4401	0.4420

TABLE III. Simulation results for y_e, ω, and the upper and lower spinodals, $y_{s\pm}$, for $0 \leq d \leq d_c$ (a) Standard diffusion; (b) modified diffusion.

d	y_{s-}	y_e	y_{s+}	ω
(a) Standard diffusion treatment				
0.00	0.000	0.4404	0.500	5.23
0.05	0.426	0.4870	0.515	6.53
0.10	0.512	0.5238	0.531	9.30
0.11	0.522	0.5299	0.535	10.15
0.12	0.532	0.5363	0.539	11.13
(b) Modified diffusion treatment				
0.00	0.000	0.4185	0.500	4.17
0.05	0.426	0.4807	0.515	5.35
0.10	0.512	0.5221	0.531	7.71
0.11	0.522	0.5228	0.535	8.70
0.12	0.532	0.5355	0.539	9.88

V. CONCLUSIONS

In summary, we have proposed a hybrid treatment for surface reactions where immobile and highly mobile reactants coexist. We implemented a LG description of the immobile adspecies (thus describing spatial correlations in their distribution), and a MF description of the highly mobile adspecies. In the cases considered here, the high mobility produced a well-mixed locally equilibrated adlayer of the mobile adspecies, quenching fluctuations, and inducing very strong metastability (and hysteresis) in the full LG model. This was reflected by the presence of bistability in the hybrid model. Our analysis of the monomer–dimer ($A+B_2$) surface reaction, with highly mobile A(ad) and immobile B(ad), has shown that spatial correlations in the B(ad)-distribution do not significantly modify features of the MF phase diagram (for a system with macroscopic spatial homogeneity), such as bistability and cusp bifurcations. However detailed fluctuation behavior in the vicinity of such bifurcations, and the occurrence of continuous poisoning transitions, is quite distinct from MF behavior. We also show how to treat macroscopic spatial inhomogeneities, such as chemical waves, within this hybrid formalism. This allows, e.g., determination of the equistability point in the bistable region (the kinetic analog of Maxwell's construction). The associated novel parallel simulation procedure for incorporating atomic scale correlations into the analysis of macroscopic spatial phenomena is quite general, well suited to parallel computer architectures, and effectively limited only by availability of detailed energetic and mechanistic information characterizing atomic reaction processes.

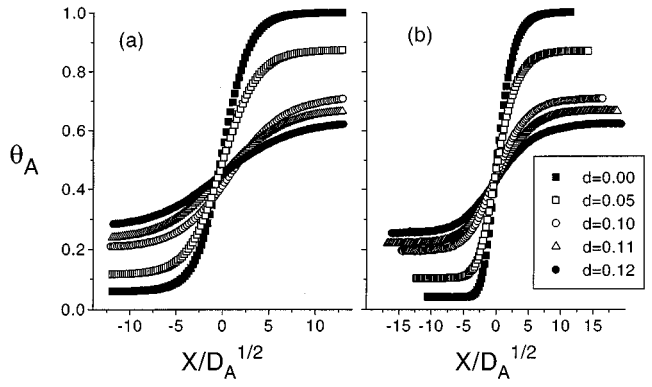

FIG. 8. Chemical wave profiles at $y=y_e$ for various d. Note the increasing width of the wave profile as $d \to d_c$: (a) standard diffusion; (b) modified diffusion.

ACKNOWLEDGMENTS

This work was supported by the Division of Chemical Sciences, Office of Basic Energy Sciences, of the Department of Energy (USDOE). Ames Laboratory is operated for the USDOE by Iowa State University under Contract No. W-7405-Eng-82.

APPENDIX A: HIERARCHIC RATE EQUATIONS AND APPROXIMATIONS

Here we briefly discuss the exact hierarchic rate equations for the hybrid model, and describe site- and pair-approximations to these. These hierarchic equations for general LG models describe the evolution of probabilities (or concentrations) for various subconfigurations of sites. In the hybrid model, some simplifications arise due to the feature that the A(ad) are strictly randomly distributed. For convenience, below we present the probabilities of various configurations by the configurations themselves. Thus one has $A=\theta_A$, $B=\theta_B$, and E, AB, BBA, $\overset{A}{BB}$, etc. represent the probabilities of an empty site, an A(ad)–B(ad) pair, linear and bent B(ad)–B(ad)–A(ad) triples, etc.

It is instructive to consider first the general LG model for the $A+B_2$ reaction, where there are three single site configuration probabilities, A, B, and E, and six distinct pair configurations probabilities, AA, BB, EE, AB, AE, and BE. (Note that by inversion symmetry $BE=EB$, etc.) However, there are also conservation of probability conditions, $A+B+E=1$, and $AA+BB+EE+2AB+2AE+2BE=1$. Also the single site probabilities can be determined from the pair probabilities via the relations $AB+AE+AA=A$, $AB+EB+BB=B$, and $AE+BE+EE=E$. In the hybrid model, further relationships exist. To see this, introduce a state Z describing a site is *not* occupied by B. Then one has $Z+B=1$, $ZZ+2\ ZB+BB=1$, etc. Clearly, a Z-site can be either empty, with probability (E/Z), or occupied by A, with probability (A/Z). Also note that since A(ad) are randomly distributed, one has

$$AA=ZZ\left(\frac{A}{Z}\right)^2,\quad EE=ZZ\left(\frac{E}{Z}\right)^2,\quad AB=ZB\left(\frac{A}{Z}\right)$$

and

$$EB=ZB\left(\frac{E}{Z}\right). \tag{A1}$$

The above discussion shows that the state of single site and pair configurations in the hybrid model is fully (and conveniently) described by the three independent quantities A, B, and ZB. The exact rate equations for these are

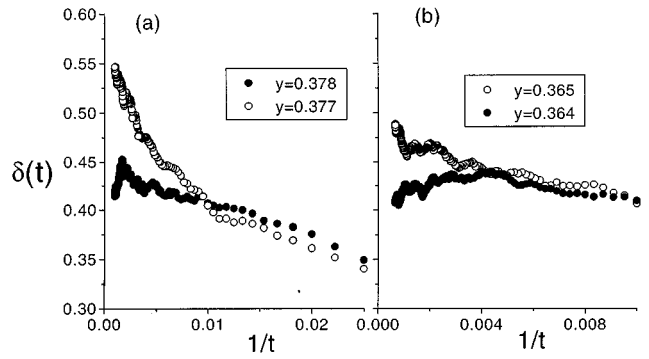

FIG. 9. Epidemic analysis results for $\delta(t)$: (a) hybrid model, $y_1=0.3775\pm0.0005$; (b) immobile model, $y_1=0.3645\pm0.0005$.

$$\frac{dA}{dt}=yE-4kAB-dA, \quad \frac{dB}{dt}=2yEE-4kAB$$

and

$$\frac{dBB}{dt}=\frac{(1-y)}{2}(EE+4^{E}_{BE}+2BEE)-2k(BBA+2^{A}_{BB}), \tag{A2}$$

where $k=1$ in our study. The terms on the right-hand side simply account for all possible ways to create or destroy the configurations of interest by adsorption, desorption, or reaction. In the site-approximation, one simply factorizes all configuration probabilities in terms of single site probabilities. This closes the first two equations, and produces the standard MF approximation to the $A+B_2$ LG reaction model. In the pair-approximation, these equations are closed by factoring the triplet configuration probabilities as $IJK=(IJ\cdot JK/J)$, where I,J,K, are any of A,B,Z,E, and then by applying Eq. (6) together with conservation of probability conditions.

APPENDIX B: THE *B*-POISONING TRANSITION

One feature of the hybrid model, characteristic also of the full LG model, is the appearance of a B-poisoning transition. For $d=0$, we determine precisely here the location, $y=y_1$, of this transition, as well as the associated critical exponents, and compare with behavior in the corresponding immobile LG model. We utilize an ''epidemic analysis,'' which involves monitoring the evolution of an empty patch embedded in a B-poisoned background.[11] The quantity of interest is the epidemic survival probability, $P_s(t)$. That is, $P_s(t)$ is the probability that at time t the lattice has not completely poisoned with B. For $y<y_1$, the $t\to\infty$ asymptotic survival probability approaches zero exponentially, while for $y>y_1$, it is nonzero. At $y=y_1$, the survival probability is expected to scale like $P_s(t)\sim t^{-\delta}$, as $t\to\infty$. To precisely determine the exponent, δ, it is useful to consider the ''local exponent'' defined as[11]

$$\delta(t)=\frac{\log[P_s(t)/P_s(t/5)]}{\log(5)}. \tag{B1}$$

Thus, as $t\to\infty$, the local exponent should approach zero for $y>y_1$, and it should diverge for $y<y_1$. At $y=y_1$ it can be shown[11] that, for large t, $\delta(t)\sim\delta+a/t$. Figure 9(a) shows $\delta(t)$ vs $1/t$ for the hybrid model bending downward towards zero for $y=0.378$ (indicating that $y_1<0.378$), and bending upward for $y=0.377$ (indicating that $y_1>0.377$). Therefore we conclude that $y_1=0.3775\pm0.0005$. The data is also consistent with a value of $\delta=0.452$ associated with the universality class of Reggeon field theory.[11] We performed an identical analysis for the immobile LG model with $k=1$ [Fig. 9(b)] indicating that $y_1=0.3645\pm0.0005$ (and $\delta=0.452$).

These results reveal a small but definite difference between the values of y_1 for the hybrid and immobile LG models. Since the only difference between these models is the treatment of A(ad), and since θ_A vanishes at the B-poisoning transition, one might have expected that the values of y_1 would be the same. However, we shall see that although θ_A vanishes at $y=y_1$, the ''local concentration,'' $\theta_A^{\rm loc}=\theta_A/\theta_Z$, of A(ad) on non-B or Z-sites remains finite. We believe this produces the difference in model behavior. From simulations, we find that $\theta_A^{\rm loc}$ approaches about 0.127 for the hybrid model, and 0.005 for the immobile model, as $y\to y_1$. Similarly, in the pair approximation, the location of the B-poisoning transition in the hybrid model of $y_1=0.2374$, differs slightly from the immobile LG model value of $y_1=0.2340$. We find that the pair approximation estimate of $\theta_A^{\rm loc}$ approaches about 0.07, as $y\to y_1$, in both models.

APPENDIX C: FLUCTUATIONS IN ADSPECIES COVERAGES

We start by considering the rms fluctuations in coverage for adspecies J in a translationally invariant surface reaction model on a finite lattice of N sites with periodic boundary conditions. Now introduce a site occupation number $n_{\mathbf{l}}$ which is equal to one if site $\mathbf{l}$ is occupied by J, and zero otherwise. Then we can write the coverage as $\theta_J=(1/N)\Sigma_{\mathbf{l}}n_{\mathbf{l}}$, so $\langle\theta_J\rangle=\langle n_{\mathbf{l}}\rangle$, for all $\mathbf{l}$. The fluctuations are given by

$$\begin{aligned}\Delta_J^2=\langle(\theta_J-\langle\theta_J\rangle)^2\rangle&=\left\langle\frac{1}{N^2}\sum_{\mathbf{l},\mathbf{l}'}(n_{\mathbf{l}}-\langle n_{\mathbf{l}}\rangle)(n_{\mathbf{l}'}-\langle n_{\mathbf{l}'}\rangle)\right\rangle\\&=\frac{1}{N^2}\sum_{\mathbf{l},\mathbf{l}'}\langle(n_{\mathbf{l}}-\langle n_{\mathbf{l}}\rangle)(n_{\mathbf{l}'}-\langle n_{\mathbf{l}'}\rangle)\rangle\\&=\frac{1}{N^2}\sum_{\mathbf{l},\mathbf{l}'}C_{JJ}(\mathbf{l},\mathbf{l}'),\end{aligned} \tag{C1}$$

where $C_{JJ}(\mathbf{l},\mathbf{l}')=\langle n_{\mathbf{l}}n_{\mathbf{l}'}\rangle-\langle\theta_J\rangle^2$ is the species J pair-correlation function.

For a *random distribution of adspecies*, we have $\langle n_{\mathbf{l}}n_{\mathbf{l}'}\rangle=\langle\theta_J\rangle^2$ for $\mathbf{l}\neq\mathbf{l}'$. For $\mathbf{l}=\mathbf{l}'$, note that $n_{\mathbf{l}}^2=n_{\mathbf{l}}$ so that $\langle n_{\mathbf{l}}n_{\mathbf{l}}\rangle=\langle\theta_J\rangle$. Now the pair-correlation function becomes $C_{JJ}(\mathbf{l},\mathbf{l}')=\langle\theta_J\rangle(1-\langle\theta_J\rangle)\delta_{\mathbf{l},\mathbf{l}'}$ so

$$\Delta_J^2=\frac{1}{N^2}\sum_{\mathbf{l},\mathbf{l}'}\langle\theta_J\rangle(1-\langle\theta_J\rangle)\delta_{\mathbf{l},\mathbf{l}'}=\frac{\langle\theta_J\rangle(1-\langle\theta_J\rangle)}{N}. \tag{C2}$$

APPENDIX D: THE MODIFIED DIFFUSIVE FLUX

For a linear lattice, let $[M_i]$ denote the probability that site i is occupied by species $M=A$, B, or E. Also let

$[M_iN_{i+1}]$ denote the probability that site i is occupied by species M, and site $i+1$ is occupied by species N. Then for the one-dimensional $A+B_2$ LG reaction model where A(ad) has hop rate h, the net diffusive flux of A(ad) *from* site i *to* site $i+1$ is given by

$$J_{i\to i+1}=h([A_iE_{i+1}]-[E_iA_{i+1}])$$
$$=-h([A_{i+1}]-[A_i])+h([B_iA_{i+1}]-[A_iB_{i+1}]), \tag{D1}$$

where we have used the relations $[A_iE_{i+1}]+[A_iB_{i+1}]+[A_iA_{i+1}]=[A_i]$ and $[E_iA_{i+1}]+[B_iA_{i+1}]+[A_iA_{i+1}]=[A_{i+1}]$. Ignoring all spatial correlations (so one can write $[M_iN_{i+1}]=[M_i][N_{i+1}]$), and defining $\nabla[M_i]=[M_{i+1}]-[M_i]$, we obtain

$$J_{i\to i+1}=-h\nabla[A_i]+h([B_i]\nabla[A_i]-[A_i]\nabla[B_i]). \tag{D2}$$

It is trivial to generalize this analysis to a two-dimensional square lattice. Taking a continuum limit for slowly varying adspecies concentrations, where $aJ_{j\to j+1}\to J_x$, $a^2h\to D_A$, and $a^{-1}\Delta\to\partial/\partial x$, yields the expressions given in Sec. IV A.

Noted added in proof. It should be emphasized that the ''modified diffusive flux'' (D2) corresponds to treating the B(ad) as a randomized and (highly) *dynamic* background through which A(ad) diffuses. Instead, treating B(ad) as a randomized and *static* background implies that $J_A=-D_A(\theta_B)\nabla\theta_A$, where $D_A(p)$ describes diffusion on a square lattice with a fraction p of the sites blocked. Results from percolation theory show that $D_A(p)=0$ for $p>p_c\approx 0.41$, and below we use the approximation $D_A(p)\propto(p_c-p)^{1.3}$ for $p<p_c$. Certainly, there is some B(ad) dynamics due to adsorption and reaction, suggesting that the ''dynamic'' rather than the ''static'' picture might better describe behavior in the LG-reaction model. Indeed, implementing this ''percolative diffusive flux'' in the hybrid model with $d=0$ yields $y_e=0.3978$ (simulation), 0.3971 (pair approximation), 0.4074 (site approximation). Thus estimates of y_e in Table II using the modified diffusive flux appear to better match the estimated $h\to\infty$ LG-model value of 0.423.

[1] Y. Kuramoto, *Chemical Oscillations, Waves, and Turbulence* (Springer, Berlin, 1984).
[2] G. Ertl, Adv. Catal. **37**, 213 (1991); R. Imbihl, Prog. Surf. Sci. **44**, 185 (1994).
[3] R. Imbihl and G. Ertl, Chem. Rev. **95**, 697 (1995).
[4] R. M. Ziff, E. Gulari, and Y. Barshad, Phys. Rev. Lett. **50**, 2553 (1986).
[5] J. W. Evans and M. Sabella, in *Trends in Statistical Physics* (Council of Scientific Research Integration, Trivandrum, India, 1995), Vol. 1; J. W. Evans, Langmuir **7**, 2514 (1991).
[6] B. J. Brosilow and R. M. Ziff, Phys. Rev. A **46**, 4534 (1992); E. V. Albano, Appl. Phys. A **54**, 1 (1992).
[7] T. Tome and R. Dickman, Phys. Rev. E **47**, 948 (1993).
[8] J. W. Evans and T. R. Ray, Phys. Rev. E **50**, 4302 (1994).
[9] R. M. Ziff and B. J. Brosilow, Phys. Rev. A **46**, 4630 (1992).
[10] M. Silverberg and A. Ben-Shaul, J. Chem. Phys. **87**, 3178 (1989); H. C. Kang, T. A. Jachimowiski, and W. H. Weinberg, *ibid*. **93**, 1418 (1990); K. A. Fitchthorn and W. H. Weinberg, Langmuir **7**, 2539 (1991).
[11] I. Jensen, H. Fogedby, and R. Dickman, Phys. Rev. A **41**, 3411 (1990).
[12] J. W. Evans and M. S. Miesch, Phys. Rev. Lett. **66**, 833 (1991).
[13] M. Dumont, M. Poriaux, and R. Dagonnier, Surf. Sci. **169**, L307 (1986); M. Dumont, P. Dufour, B. Sente, and R. Dagonnier, J. Catal. **122**, 95 (1990).
[14] H. P. Kaukonen and R. M. Niemenen, J. Chem. Phys. **91**, 4380 (1989); M. Ehsasi, M. Matloch, J. H. Block, K. Christmann, F. S. Rys, and W. Hirschwald, *ibid*. **91**, 4949 (1989).
[15] D. S. Sholl and R. T. Skodje, Surf. Sci. **334**, 295 (1995).
[16] J. W. Evans, J. Chem. Phys. **98**, 2463 (1993).
[17] J. W. Evans, J. Chem. Phys. **97**, 572 (1992).
[18] W. E. Schiesser, *The Numerical Method of Lines* (Academic, San Diego, 1991).
[19] H. Spohn, *Large Scale Dynamics of Interacting Particles* (Springer, Berlin, 1991).
[20] R. Dickman, Phys. Rev. A **34**, 4246 (1986).